# **Multi-Source Error Comprehensive Suppression Methods for Magnetic Gradient Tensor Detection System**

# Wang Minkang

The 36th Research Institute of China Electronics Technology Group Corporation, Jiaxing, China wangminkang@cug.edu.cn

Abstract: Accurate real-time magnetic detection is crucial for achieving reliable geomagnetic matching navigation. Compared to traditional magnetic parameters (total field, vector components, and gradients), Magnetic Gradient Tensor (MGT) measurements offer superior spatial resolution, enhanced antiinterference capability, and richer information content. MGT data are typically acquired using fluxgate sensor arrays; however, manufacturing tolerances, processing limitations, and inherent signal conditioning circuit imperfections introduce multiple error sources into the measurement system. To address these challenges, this paper analyzes three primary error sources within the detection system: intrinsic fluxgate sensor errors, inter-sensor misalignment errors within the array, and misalignment errors between the inertial navigation system (INS) and the fluxgate array. A comprehensive error calibration methodology for the MGT detection system is proposed. This method establishes corresponding error calibration models based on the characteristics of each error type, identifies relevant constraint relationships, and determines the solution methods for calibration parameters to achieve final error calibration. To validate the effectiveness of the proposed method, an experimental platform based on a non-magnetic turntable was constructed for error calibration experiments. The results demonstrate that the proposed method: Reduces the standard deviation of the computed total field data from fluxgates from 54.36-175.06 nT to below 2 nT, Decreases the Root Mean Square (RMS) error of triaxial readings between individual fluxgates from 301.96-29.06 nT to below 45 nT, and lowers the standard deviation of coordinate-transformed fluxgate triaxial readings from 2,317.77-3,355.33 nT to below 580 nT.

Keywords: Magnetic Gradient Tensor, Fluxgate Sensor, Error Calibration

# 1. Introduction

Geomagnetic matching navigation has been widely applied in numerous fields, including geophysical exploration, cruise missile guidance, and anti-submarine warfare [1-5], owing to its advantages of concealment and passivity. The utilization of Magnetic Gradient Tensor (MGT) detection systems for acquiring magnetic information in geomagnetic matching navigation offers unique advantages, including high spatial resolution, strong anti-interference capability, and information richness [6]. However, the measurement accuracy of MGT—and consequently the navigation performance—can be compromised by several error sources within the MGT detection system. These include intrinsic fluxgate sensor errors, misalignment errors between fluxgate sensors, and misalignment errors between INS and fluxgate sensors [7, 8]. Therefore, rigorous error calibration is an essential step in achieving high-precision geomagnetic matching navigation based on this technology.

Intrinsic fluxgate sensor errors within MGT detection systems primarily include triaxial non-orthogonality errors, zero bias errors, and scale factor errors [9]. Current calibration methods for these errors fall into two categories: auxiliary vector calibration and independent scalar calibration. The principle of the first one involves comparing the fluxgate readings with reference magnetic field data generated by a constant magnetic field reference device or measurements from high-precision scalar magnetometers. By minimizing the discrepancy between these readings, the fluxgate errors are corrected. For instance, Ren et al. [10] established an error calibration model where readings from the target sensor were input into the model and compared against the magnetic field generated by the reference device. A least-squares algorithm was then employed to solve for the calibration parameters in the model. While such methods offer straightforward procedures, their accuracy is significantly compromised by multicollinearity in magnetic measurement data and the presence of outliers, which degrade the precision

of least-squares solutions. This second one leverages the trajectory characteristics of fluxgate measurements during free rotation in a stable geomagnetic field. For example, the ellipsoid fitting method <sup>[11]</sup> transforms fluxgate error calibration into an ellipsoid fitting problem under the constraint that ideal fluxgate measurements during vertical-axis rotation should form an elliptical trajectory. Although eliminating the need for external apparatus, this method lacks cross-validation mechanisms. Even when measurement data conform to theoretical trajectory characteristics, the computed total magnetic field may still exhibit significant deviation from ground-truth values due to the absence of reference validation.

Misalignment errors between fluxgate sensors refer to the non-parallel alignment of triaxial sensors within an MGT measurement array during installation. This inconsistency causes measured magnetic vector data to reside in divergent coordinate systems, thereby introducing errors in MGT calculations. Such errors can be corrected using constraints derived from homogeneous measurements across vector sensors. For instance, Yan et al. [12] established an objective function based on the comparative relationship of corrected fluxgate readings, transforming the error calibration into an optimization problem. Kubík et al. [13] acquired multiple fluxgate readings by reorienting the sensor array in a stable geomagnetic field. They formulated nonlinear equations under the constraint that ideal fluxgate outputs must be consistent across sensors, solving these equations via the real root isolation method to calibrate inter-sensor misalignment. While these methods are conceptually straightforward and operationally feasible, their efficacy is highly dependent on the optimization algorithm's performance.

Misalignment errors between INS and fluxgate sensors arise from imprecise triaxial alignment during installation, leading to coordinate transformation errors when projecting magnetic measurements into the geographic frame. For such errors between heterogeneous vector sensors, two primary calibration approaches exist: External-Reference Calibration and Internal-Reference Calibration. The first one relies on precision equipment. For example, Pang et al. [14] proposed a calibration technique using a non-magnetic hexahedral frame to align fluxgate arrays with INS. The core idea involves stepwise calibration of discrepancies between fluxgate/INS axes and the hexahedral frame's coordinate system. However, accuracy is constrained by the precision of auxiliary devices. This sencond one uses one internal vector sensor as a reference. Li et al. [15] leveraged the invariance of vector dot products under coordinate rotation, proposing a dot-product invariant method to correct misalignment without external apparatus. Nevertheless, it faces challenges in defining robust objective functions for heterogeneous sensors.

In practical mgt detection systems, the three aforementioned error sources coexist and require simultaneous integrated calibration. Addressing the limitations of existing research, this study proposes a comprehensive error calibration methodology for mgt systems. The primary contributions are summarized as follows:

- (1) We establish dedicated calibration models for three error categories above.
- (2) We propose the corresponding calibration methodology. Especially, for ins-fluxgate misalignment, we provide theoretical proof of an inherent constraint relationship between heterogeneous sensor data streams, enabling robust parameter solving without external references.
- (3) A non-magnetic turntable-based experimental platform was constructed, and error calibration experiments were conducted to validate the effectiveness of the proposed method.

The remainder of this paper is organized as follows: section ii introduces fundamental principles of mgt detection. Section III details the proposed methodology's theoretical framework. Section IV presents experimental validation through field tests. Finally, Conclusions are drawn in Section V.

# 2. Preliminaries of magnetic gradient tensor detection

## 2.1 Principle of magnetic gradient tensor

The MGT matrix G is defined as the spatial rate of change of the magnetic vector B along the three mutually perpendicular axes of a Cartesian coordinate system. Its mathematical expression is given by [16]:

$$G = \nabla B = \begin{bmatrix} \frac{\partial B_{x}}{\partial x} & \frac{\partial B_{y}}{\partial x} & \frac{\partial B_{z}}{\partial x} \\ \frac{\partial B_{x}}{\partial y} & \frac{\partial B_{y}}{\partial y} & \frac{\partial B_{z}}{\partial y} \\ \frac{\partial B_{x}}{\partial z} & \frac{\partial B_{y}}{\partial z} & \frac{\partial B_{z}}{\partial z} \\ \frac{\partial B_{x}}{\partial z} & \frac{\partial B_{y}}{\partial z} & \frac{\partial B_{z}}{\partial z} \end{bmatrix} = \begin{bmatrix} B_{xx} & B_{xy} & B_{zz} \\ B_{xx} & B_{yy} & B_{zz} \\ B_{zx} & B_{zy} & B_{zz} \end{bmatrix}$$

$$(1)$$

Where  $\nabla$  denotes the Hamilton operator. The background geomagnetic field—primarily originating from deep-source components—typically exhibits negligibly small magnetic gradient values. This implies that background interference can be disregarded during investigations and detection of the MGT. Furthermore, as established by Maxwell's equations, in source-free space, the divergence and curl of the magnetic field both vanish:

$$\begin{cases}
\nabla \cdot \mathbf{B} = \frac{\partial B_x}{\partial x} + \frac{\partial B_y}{\partial y} + \frac{\partial B_z}{\partial z} = 0 \\
\nabla \times \mathbf{B} = \begin{vmatrix} i & j & k \\ \frac{\partial}{\partial x} & \frac{\partial}{\partial y} & \frac{\partial}{\partial z} \\
B_x & B_y & B_z
\end{vmatrix} = 0
\end{cases} \tag{2}$$

Expanding the above expression, it can be deduced that the components of the MGT matrix G satisfy the following relationships:

$$\begin{cases} B_{xy} = B_{yx} \\ B_{xz} = B_{zx} \\ B_{yz} = B_{zy} \\ B_{xx} + B_{yy} + B_{zz} = 0 \end{cases}$$
(3)

Based on these identities, G contains nine components but only five are independent. Furthermore, G is a real symmetric matrix and can be expressed as:

$$G = \begin{bmatrix} B_{xx} & B_{xy} & B_{xz} \\ B_{xy} & B_{yy} & B_{yz} \\ B_{xz} & B_{yz} & -B_{xx} - B_{yy} \end{bmatrix}$$
(4)

## 2.2 Magnetic gradient tensor measurement array

The cross-shaped MGT measurement array is widely adopted due to its structural simplicity and high measurement accuracy <sup>[17]</sup>. As illustrated in Figure 1, the array comprises four fluxgate sensors labeled sequentially as S1, S2, S3, and S4.

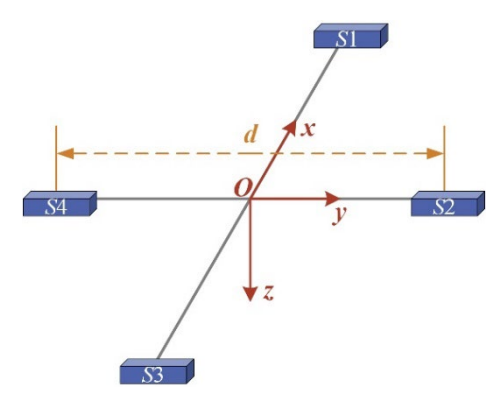


Figure 1: Schematic of cross-shaped MGT measurement array

Where sensors S1 and S3 are positioned along the x-axis of the measurement coordinate system, separated by a baseline distance d. Sensors S2 and S4 are positioned along the y-axis, equally separated by the baseline distance d. The origin O of the measurement array defines the MGT measurement point. All sensor coordinate systems are aligned with the array's global coordinate system.

The magnetic gradient tensor matrix  $G_m$  at point O is derived by approximating spatial derivatives through differential measurements between fluxgate sensor readings over short distances. For a cross-shaped array,  $G_m$  is computed as:

$$G_{m} = \frac{1}{d} \begin{bmatrix} B_{x}^{S1} - B_{x}^{S3} & B_{y}^{S1} - B_{y}^{S3} & B_{z}^{S1} - B_{z}^{S3} \\ B_{y}^{S1} - B_{y}^{S3} & B_{y}^{S2} - B_{y}^{S4} & B_{z}^{S2} - B_{z}^{S4} \\ B_{z}^{S1} - B_{z}^{S3} & B_{z}^{S2} - B_{z}^{S4} & B_{x}^{S3} + B_{y}^{S4} - \left(B_{x}^{S1} + B_{y}^{S2}\right) \end{bmatrix}$$

$$(5)$$

Where  $B_i^{Si}$  denotes the magnetic filed reading along the *j*-axis of sensor Si.

# 3. Proposed Error calibration method for magnetic gradient tensor detection system

The developed MGT detection system incorporates an INS rigidly connected to the magnetic tensor measurement array. This configuration enables real-time attitude capture of fluxgate sensors, facilitating attitude calibration to unify all fluxgate readings into a common geomagnetic coordinate system. Consequently, the system exhibits three primary error sources:i) Intrinsic fluxgate sensor errors. ii) Misalignment errors between fluxgate sensors. iii) Misalignment errors between INS and fluxgate sensors.

#### 3.1 Intrinsic fluxgate sensor errors

#### 3.1.1 Error calibration model

Each fluxgate sensor comprises three orthogonal magnetic sensing axes (designated x, y, z) forming its measurement coordinate frame. However, mechanical imperfections and electrical limitations introduce three intrinsic error types: Triaxial non-orthogonal error, Scale factor error and Zero offset error.

As depicted in Figure 2, two coordinate frames are defined: an ideal orthogonal reference frame (O-xyz) and a fluxgate measurement frame ( $O_m$ - $x_my_mz_m$ ).

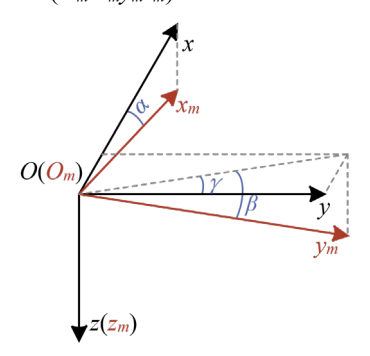


Figure 2: Non-orthogonality of fluxgate sensor triaxial axes

Assuming that the origin of the reference frame coincides with the fluxgate measurement frame, the z-axis is in the same direction, and the xOz plane coincides with the  $x_mOz_m$  plane. the non-orthogonal relationship is parameterized by three angles: where  $\alpha$  denotes angle between  $x_m$ -axis and x-axis,  $\beta$  denotes angle between  $x_m$ -axis and xOy plane and  $\gamma$  denotes angle between the projection of  $y_m$ -axis onto xOy plane and y-axis. Then the coordinate transformation matrix for correcting non-orthogonal error is given by:

$$\begin{bmatrix} x \\ y \\ z \end{bmatrix} = \begin{bmatrix} \cos \alpha & 0 & \sin \alpha \\ \cos \beta \cos \gamma & \cos \alpha \sin \gamma & \sin \beta \\ 0 & 0 & 1 \end{bmatrix} \begin{bmatrix} x_m \\ y_m \\ z_m \end{bmatrix}$$
 (6)

Futhermore, Incorporating scale factors  $k_x$ ,  $k_y$ ,  $k_z$  and zero offsets  $\mathbf{h} = [h_x, h_y, h_z]^T$ , Then the conversion relationship between the measured value  $\mathbf{B}_m = [B_{mx}, B_{mx}, B_{mx}]^T$  of flux gates and the true magnetic  $\mathbf{B} = [B_x, B_y, B_z]^T$  can be represented by (7), that is:

$$\begin{bmatrix} B_{x} \\ B_{y} \\ B_{z} \end{bmatrix} = \begin{bmatrix} \cos \alpha & 0 & \sin \alpha \\ \cos \beta \cos \gamma & \cos \alpha \sin \gamma & \sin \beta \\ 0 & 0 & 1 \end{bmatrix}^{-1} \begin{bmatrix} k_{x} \\ k_{y} \\ k_{z} \end{bmatrix} \begin{bmatrix} B_{mx} - h_{x} \\ B_{my} - h_{y} \\ B_{mz} - h_{z} \end{bmatrix}$$
(7)

Let

$$\mathbf{Q} = \begin{bmatrix} \cos \alpha & 0 & \sin \alpha \\ \cos \beta \cos \gamma & \cos \alpha \sin \gamma & \sin \beta \\ 0 & 0 & 1 \end{bmatrix}^{-1} \begin{bmatrix} k_x \\ k_y \\ k_z \end{bmatrix} = \begin{bmatrix} q_{11} & 0 & q_{13} \\ q_{21} & q_{22} & q_{23} \\ 0 & 0 & q_{33} \end{bmatrix}$$
(8)

Therefore, (7) can be expressed as:

$$\boldsymbol{B} = \boldsymbol{Q} \left( \boldsymbol{B}_{m} - \boldsymbol{h} \right) \tag{9}$$

(9) Constitutes the calibration model for intrinsic fluxgate sensor errors, where the nine parameters contained in matrices Q and vector h represent the calibration parameters.

## 3.1.2 Error calibration method

Based on (9), the square of the magnetic total field can be expressed as:

$$B^{2} = \boldsymbol{B}^{\mathrm{T}}\boldsymbol{B} = (\boldsymbol{B}_{m} - \boldsymbol{h})^{\mathrm{T}}\boldsymbol{Q}^{\mathrm{T}}\boldsymbol{Q}(\boldsymbol{B}_{m} - \boldsymbol{h})$$

$$(10)$$

This can be rearranged into a product form composed of a vector of fluxgate measurements and a vector of nine calibration parameters:

$$B^2 = mk \tag{11}$$

Where

$$\mathbf{m} = \left[ B_{mx}^2, B_{my}^2, B_{mz}^2, B_{mx} B_{my}, B_{mx} B_{mz}, B_{my} B_{mz}, B_{mx}, B_{my}, B_{mz}, 1 \right]$$
(12)

$$\mathbf{k} = \begin{bmatrix} q_{11}^2 + q_{21}^2, q_{22}^2, q_{13}^2 + q_{23}^2 + q_{33}^2, 2q_{21}q_{22}, 2(q_{11}q_{13} + q_{21}q_{23}), 2q_{22}q_{23}, \\
-2(q_{11}^2 + q_{21}^2)h_x - 2q_{21}q_{22}h_y - 2(q_{11}q_{13} + q_{21}q_{23})h_z, -2q_{21}q_{22}h_x - 2q_{22}^2h_y \\
-2q_{22}q_{23}h_z, -2(q_{11}q_{13} + q_{21}q_{23})h_x - 2q_{22}q_{23}h_y - 2(q_{13}^2 + q_{23}^2 + q_{33}^2)h_z, \\
(q_{11}^2 + q_{21}^2)h_x^2 + q_{22}^2h_y^2 + (q_{133}^2 + q_{23}^2 + q_{33}^2)h_z^2 + 2q_{21}q_{22}h_xh_y + 2q_{22}q_{23}h_yh_z \\
+2(q_{11}q_{13} + q_{21}q_{23})h_xh_z \end{bmatrix}^{\mathsf{T}}$$
(13)

In a stable and uniform geomagnetic field, if  $N (N \ge 10)$  groups of distinct fluxgate measurements  $m_1$ ,  $m_2$ , ...,  $m_N$  are obtained by altering the fluxgate's attitude, and the corresponding magnetic total field values  $B_1, B_2, ..., B_N$  are simultaneously acquired using an optical pumping magnetometer, the parameter vector k can be estimated via the least squares method:

$$\hat{\boldsymbol{k}} = \left(\boldsymbol{m}_c^{\mathrm{T}} \boldsymbol{m}_c\right)^{-1} \boldsymbol{m}_c^{\mathrm{T}} \boldsymbol{H} \tag{14}$$

Where  $\mathbf{m}_c = [\mathbf{m}_1, \mathbf{m}_2, ..., \mathbf{m}_N]^T$  and  $\mathbf{H} = [B_1^2, B_2^2, ..., B_N^2]^T$  denotes the matrix composed of magnetic measurement data. Through (14), the calibration parameters can be inversely solved, thereby completing the calibration of its intrinsic errors.

## 3.2 Misalignment errors between fluxgate sensors

#### 3.2.1 Error calibration model

The non-parallelism of sensitive axes between fluxgate sensors induces coordinate system inconsistencies, leading to significant errors in tensor measurements.

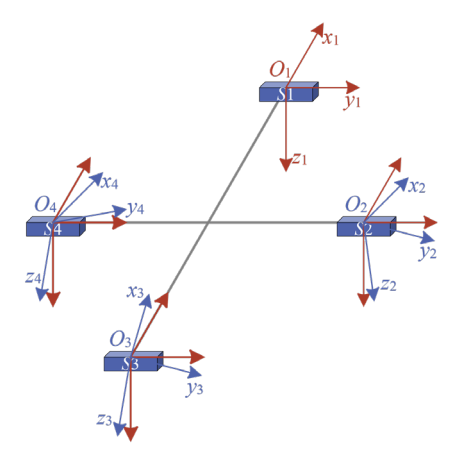


Figure 3: Misalignment between fluxgate coordinate frame and reference coordinate system.

To characterize the misalignment errors among an array of fluxgate sensors, the coordinate system of the u-th sensor (u = 1, 2, 3, 4) is denoted as  $O_u - x_u y_u z_u$ , as illustrated in Figure 3. These four coordinate systems are not mutually aligned. Any three-dimensional coordinate system can be aligned to another via Euler rotations [18]. By defining the first fluxgate's coordinate system ( $O_1 - x_1 y_1 z_1$ ) as the reference, the systems of the other three fluxgates can be aligned to it through a sequence of Euler rotations. Specifically, to align the coordinate system  $O_v - x_v y_v z_v$  (v = 2, 3, 4) to  $O_1 - x_1 y_1 z_1$ , it is assumed to first rotate by an angle  $\alpha_v$  about the  $x_v$ -axis (following the right-hand rule), then by  $\beta_v$  about the  $y_v$ -axis, and finally by  $\gamma_v$  about the  $z_v$ -axis. The Euler rotation matrix describing this process is:

$$R(\alpha_{v}, \beta_{v}, \gamma_{v}) = R_{z}(\gamma_{v})R_{y}(\beta_{v})R_{x}(\alpha_{v})$$

$$= \begin{bmatrix} \cos \gamma_{v} & -\sin \gamma_{v} & 0 \\ \sin \gamma_{v} & \cos \gamma_{v} & 0 \\ 0 & 0 & 1 \end{bmatrix} \begin{bmatrix} \cos \beta_{v} & 0 & \sin \beta_{v} \\ 0 & 1 & 0 \\ -\sin \beta_{v} & 0 & \cos \beta_{v} \end{bmatrix} \begin{bmatrix} 1 & 0 & 0 \\ 0 & \cos \alpha_{v} & -\sin \alpha_{v} \\ 0 & \sin \alpha_{v} & \cos \alpha_{v} \end{bmatrix}$$

$$= \begin{bmatrix} \cos \beta_{v} \cos \gamma_{v} & \sin \alpha_{v} \sin \beta_{v} \cos \gamma_{v} - \cos \alpha_{v} \sin \gamma_{v} \\ \cos \beta_{v} \sin \gamma_{v} & \sin \alpha_{v} \sin \beta_{v} \sin \gamma_{v} + \cos \alpha_{v} \cos \gamma_{v} \\ -\sin \beta_{v} & \sin \alpha_{v} \cos \beta_{v} \end{bmatrix}$$

$$= \cos \alpha_{v} \sin \beta_{v} \cos \gamma_{v} + \sin \alpha_{v} \sin \gamma_{v}$$

$$\cos \alpha_{v} \sin \beta_{v} \sin \gamma_{v} - \sin \alpha_{v} \cos \gamma_{v}$$

$$\cos \alpha_{v} \sin \beta_{v} \sin \gamma_{v} - \sin \alpha_{v} \cos \gamma_{v}$$

$$\cos \alpha_{v} \cos \beta_{v} \cos \beta_{v}$$

$$(15)$$

Let  $\mathbf{B}_{v} = \begin{bmatrix} B_{vx}, B_{vy}, B_{vz} \end{bmatrix}^{T}$  be the magnetic field measured by the *v*-th fluxgate and  $\tilde{\mathbf{B}}_{v} = \begin{bmatrix} \tilde{B}_{vx}, \tilde{B}_{vy}, \tilde{B}_{vz} \end{bmatrix}^{T}$  be its value in the reference coordinate system. Their relationship is:

$$\tilde{\boldsymbol{B}}_{v} = \boldsymbol{R}(\alpha_{v}, \beta_{v}, \gamma_{v}) \boldsymbol{B}_{v} \tag{16}$$

(16) Constitutes the calibration model for misalignment errors between fluxgate sensors, with  $\alpha_{\nu}$ ,  $\beta_{\nu}$  and  $\gamma_{\nu}$  serving as its calibration parameters.

# 3.2.2 Error calibration method

In a uniform and stable magnetic field environment, if inter-fluxgate misalignment errors are absent and intrinsic errors of all fluxgate sensors have been corrected, the readings from the four fluxgate sensors should theoretically remain consistent. This implies the relationship  $\tilde{\boldsymbol{B}}_{v} = \boldsymbol{B}_{1}$ , where  $\boldsymbol{B}_{1}$  denotes the magnetic measurement from the first fluxgate. By altering the orientation of the measurement array to obtain N sets of magnetic vector data across different poses, the objective function for correcting misalignment errors between the v-th fluxgate and first fluxgate is defined as:

$$F(\alpha_{\nu}, \beta_{\nu}, \gamma_{\nu}) = \frac{1}{N} \sum_{s=1}^{N} \left\| \mathbf{R} \left( \alpha_{\nu}, \beta_{\nu}, \gamma_{\nu} \right) \mathbf{B}_{\nu}^{s} - \mathbf{B}_{1}^{s} \right\|^{2}$$

$$(17)$$

Where  $\mathbf{B}_{v}^{s}$  represents the reading of the v-th fluxgate under the s-th orientation.

Minimizing (17) yields estimates of the calibration parameters  $\alpha_{\nu}$ ,  $\beta_{\nu}$  and  $\gamma_{\nu}$ :

$$\hat{\alpha}_{v}, \hat{\beta}_{v}, \hat{\gamma}_{v} = \arg\min_{\alpha_{v}, \beta_{v}, \gamma_{v}} F(\alpha_{v}, \beta_{v}, \gamma_{v})$$
(18)

(18) Constitutes a multi-objective nonlinear optimization problem. For such problems, direct analytical solutions are typically infeasible; instead, iterative numerical methods are employed to approximate optimal parameters. The Levenberg-Marquardt (LM) algorithm is a widely adopted iterative optimization technique, with its update rule given by [19]:

$$\boldsymbol{\theta}_{k+1} = \boldsymbol{\theta}_k - \left(\boldsymbol{J}_k^{\mathrm{T}} \boldsymbol{J}_k + \mu \boldsymbol{I}\right)^{-1} \boldsymbol{J}_k^{\mathrm{T}} \boldsymbol{e}_k \tag{19}$$

Where  $\theta_k$  is the vector of estimated calibration parameters at iteration k;  $e_k$  denotes the N-dimensional residual vector of the objective function values;  $J_k$  is the Jacobian matrix of  $e_k$ ;  $\mu$  is a damping hyperparameter that mitigates ill-conditioning in  $J_k^T J_k$ .

#### 3.3 Misalignment errors between inertial navigation system and fluxgate sensors

#### 3.3.1 Error calibration model

The three axes of the INS and fluxgate cannot be guaranteed to be mutually parallel. This results in a misalignment error between the INS and the fluxgate sensor.

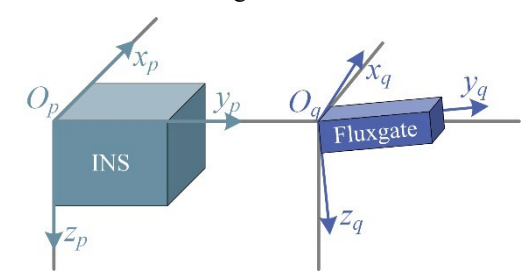


Figure 4: Coordinate systems of fluxgate and INS.

The coordinate system of the INS is defined as  $O_p$ - $x_py_pz_p$ , and that of the fluxgate is defined as  $O_q$ - $x_qy_qz_q$ . As illustrated in Figure 4, misalignment between these two coordinate systems inevitably arises due to hardware machining and installation tolerances. Using the INS coordinate system as the reference frame, the fluxgate coordinate system can be transformed to align with this reference. Assuming the coordinate system  $O_q$ - $x_qy_qz_q$  first rotates by angle  $\psi$  around the  $x_q$ -axis, then by  $\theta$  around the  $y_q$ -axis, and finally by  $\varphi$  around the  $z_q$ -axis to coincide with  $O_p$ - $x_py_pz_p$ . the Euler rotation matrix describing this alignment process is:

$$\mathbf{R}(\psi, \theta, \varphi) = \mathbf{R}_{z}(\varphi)\mathbf{R}_{v}(\theta)\mathbf{R}_{x}(\psi) \tag{20}$$

Let  $\mathbf{B}_m = [B_{mx}, B_{my}, B_{mz}]^T$  denote the magnetic vector measured by the fluxgate in its native frame (Fig. 4), and  $\mathbf{B}_t = [B_{tx}, B_{ty}, B_{tz}]^T$  represent the equivalent measurement in the INS-aligned frame. The relationship between these measurements before and after coordinate transformation is:

$$\boldsymbol{B}_{t} = \boldsymbol{R}(\boldsymbol{\psi}, \boldsymbol{\theta}, \boldsymbol{\varphi}) \boldsymbol{B}_{m} \tag{21}$$

(21) Constitutes the calibration model for misalignment errors between INS and fluxgate sensors, where the rotation angles  $\psi$ ,  $\theta$  and  $\varphi$  embedded in R are the calibration parameters.

# 3.3.2 Error calibration method

The fluxgate sensor and INS are distinct types of sensors. By utilizing the attitude data measured by the INS, the orientation of the system can be determined. An auxiliary vector field is then employed to resolve the vector field in the INS coordinate frame. Subsequently, constraints between this vector field and the magnetic vector are established to solve for the misalignment calibration parameters.

# 1) Vector Field Transformation of Attitude Data

An auxiliary vector field is assumed, which yields a measurement denoted as  $W_0$  when the INS coordinate frame coincides with the East-North-Up (ENU) orthogonal coordinate system (i.e., roll, pitch, and yaw angles are zero). When the INS undergoes attitude changes, measuring roll angle a, pitch angle b, and yaw angle c, the measurement of this auxiliary vector field is derived as:

$$\boldsymbol{W} = \boldsymbol{R}_{v}(-c)\boldsymbol{R}_{x}(-b)\boldsymbol{R}_{z}(-a)\boldsymbol{W}_{0} \tag{22}$$

Where  $R_x$ ,  $R_y$  and  $R_z$  as defined in (15). (22) accomplishes the vector field transformation of INS-measured attitude data. Here, W represents the measurement equivalent to that of a vector sensor aligned with the INS coordinate frame.

# 2) Vector Field Constraint Relationships

An arbitrary non-zero vector field with a measurement  $A = [A_x, A_y, A_z]^T$  in coordinate frame  $O_c$  is assumed. When frame  $O_c$  undergoes rotations about an arbitrary axis  $\mathbf{k} = [k_x, k_y, k_z]^T$  by angles  $\theta_1$ ,  $\theta_2$  ans  $\theta_3$ , According to Rodrigues' rotation theory [20], these measurements satisfy:

$$A_{1} = M(\theta_{1}) A = \left[ I + R_{k} \sin \theta_{1} + R_{k}^{2} \left( 1 - \cos \theta_{1} \right) \right] A$$

$$(23)$$

$$\boldsymbol{A}_{2} = \boldsymbol{M}(\theta_{2})\boldsymbol{A} = \left[\boldsymbol{I} + \boldsymbol{R}_{k}\sin\theta_{2} + \boldsymbol{R}_{k}^{2}(1-\cos\theta_{2})\right]\boldsymbol{A}$$
 (24)

$$A_3 = M(\theta_3) A = \left[ I + R_k \sin \theta_3 + R_k^2 (1 - \cos \theta_3) \right] A$$
 (25)

Where

$$\mathbf{R}_{k} = \begin{bmatrix} 0 & -k_{z} & k_{y} \\ k_{z} & 0 & -k_{x} \\ -k_{y} & k_{x} & 0 \end{bmatrix}$$
 (26)

Furthermore, since  $det(\mathbf{R}_k) = 0$ , there is:

$$\det(\mathbf{A}_{1} - \mathbf{A}, \mathbf{A}_{2} - \mathbf{A}, \mathbf{A}_{3} - \mathbf{A}) = \det\{\mathbf{R}_{k} \left[ \mathbf{f}(\theta_{1}) \mathbf{A}, \mathbf{f}(\theta_{2}) \mathbf{A}, \mathbf{f}(\theta_{3}) \mathbf{A} \right] \}$$

$$= \det(\mathbf{R}_{k}) \cdot \det[\mathbf{f}(\theta_{1}) \mathbf{A}, \mathbf{f}(\theta_{2}) \mathbf{A}, \mathbf{f}(\theta_{3}) \mathbf{A} \right]$$

$$= 0$$
(27)

Where

$$f(\theta) = I \sin \theta + R_{k} (1 - \cos \theta) \tag{28}$$

(28) Indicates the vectors  $(A_1 - A)$ ,  $(A_2 - A)$  and  $(A_3 - A)$  are linearly dependent. This implies that the terminal points of A,  $A_1$ ,  $A_2$  and  $A_3$  are coplanar. The normal vector of this plane is given by:

$$N_{A} = (A_{1} - A) \times (A_{2} - A)$$

$$= R_{k} f(\theta_{1}) A \times R_{k} f(\theta_{2}) A$$
(29)

Similarly, for another non-zero vector field with initial measurement  $\mathbf{B} = [B_x, B_y, B_z]^T$  in frame  $O_c$ , after the same rotational sequence, its measurements  $\mathbf{B}$ ,  $\mathbf{B}_1$ ,  $\mathbf{B}_2$  and  $\mathbf{B}_3$  satisfy:

$$N_{B} = (\boldsymbol{B}_{1} - \boldsymbol{B}) \times (\boldsymbol{B}_{2} - \boldsymbol{B})$$

$$= \boldsymbol{R}_{k} \boldsymbol{f}(\boldsymbol{\theta}_{1}) \boldsymbol{B} \times \boldsymbol{R}_{k} \boldsymbol{f}(\boldsymbol{\theta}_{2}) \boldsymbol{B}$$
(30)

The terminal points of B,  $B_1$ ,  $B_2$  and  $B_3$  thus lie on a plane with normal vector  $N_B$ . Expanding (29) and (30) reveals that  $N_A$  and  $N_B$  are linearly proportional, which means  $N_A$  is parallel to  $N_B$ .

# 3) Objective function

The preceding theoretical derivation establishes two fundamental conclusions: i) For any vector sensor in a stable vector field, rotating the sensor around a fixed axis results in the terminal points of its measured vector readings lying on a common plane. ii) For any two vector sensors in their respective stable vector fields with coincident coordinate system, rotating both sensors around the same fixed axis causes the terminal points of their measured vectors to lie on two mutually parallel planes. These conclusions enable the construction of the misalignment error calibration objective function.

When the INS and fluxgate rotate synchronously around the same axis, both systems acquire data at m sampling points. For the i-th sampling point, the INS records attitude angles are  $a_i$ ,  $b_i$  and  $c_i$ . According to (22), these records can be resolved into a vector field measurement:

$$W_{i} = R(-a_{i}, -b_{i}, -c_{i})W_{0}$$
(31)

Where  $W_0$  is an arbitrary non-zero auxiliary vector. We can construct the point cloud matrix  $\mathbf{D} = \begin{bmatrix} \mathbf{W}_1^{\mathrm{T}}, \mathbf{W}_2^{\mathrm{T}}, ..., \mathbf{W}_m^{\mathrm{T}} \end{bmatrix}^{\mathrm{T}}$ , then subtract the column-wise means from it to obtain the centered matrix  $D_c$ , and finally perform singular value decomposition (SVD) on  $D_c$ :

$$\mathbf{D}_{\cdot} = \mathbf{U} \sum \mathbf{V}^{\mathrm{T}} \tag{32}$$

The right singular vector  $V_{\min}$  corresponding to the smallest singular value represents the normal vector of the plane containing the terminal points of  $W_i$ . For the fluxgate, the measured vector at the i-th sampling point, denoted as  $B_i$ , is transformed into the INS coordinate frame using (21). Based on Conclusion ii, the following relationship holds:

$$V_{\min} \cdot \left[ \mathbf{R} (\psi, \theta, \varphi) \mathbf{B}_{i} - \mathbf{R} (\psi, \theta, \varphi) \mathbf{B}_{j} \right] = 0$$
(33)

The objective function for misalignment errors between INS and fluxgate sensors is thus defined as:

$$g(\psi,\theta,\varphi) = \frac{mn(m-1)}{2} \sum_{k}^{n} \sum_{i=1}^{m-1} \sum_{j=i+1}^{m} \left\{ V_{\min}^{k} \cdot \left[ \mathbf{R}(\psi,\theta,\varphi) \mathbf{B}_{i}^{k} - \mathbf{R}(\psi,\theta,\varphi) \mathbf{B}_{j}^{k} \right] \right\}^{2}$$
(34)

Where *n* represents the number of experiments. Minimizin (34) yields estimates of the calibration parameters  $\psi$ ,  $\theta$  ans  $\varphi$ :

$$\hat{\psi}, \hat{\theta}, \hat{\varphi} = \arg\min_{\psi, \theta, \phi} g\left(\psi, \theta, \varphi\right) \tag{35}$$

Substituting the optimized  $\hat{\psi}$ ,  $\hat{\theta}$  and  $\hat{\phi}$  into (21) completes the errors calibration. (35) constitutes a multi-objective nonlinear optimization problem. As in Section 3.2, the LM algorithm solves this efficiently via iterative updates.

# 4. Experimental result

The error calibration methods discussed in this chapter require a stable and uniform magnetic field environment. Consequently, all field experiments were conducted at the Yingcheng Seismic Monitoring Station of the Hubei Earthquake Agency in Hubei Province, China.

# 4.1 Filed calibration test for intrinsic fluxgate sensor errors

Within the station's absolute geomagnetic observation house, a measurement array containing four fluxgate sensors (Mag-03, Bartington Ltd.) was sequentially mounted on a non-magnetic turntable. Stepwise rotations were performed about each of the three axes of the fluxgates at 30° increments. The sensor outputs were recorded at each orientation, yielding 36 datasets per fluxgate. A commercial cesium optical-pumping magnetometer (CS-3, 0.6 pT/\dagger Hz@1 Hz sensitivity, Scintrex Ltd., Canada) was simultaneously deployed in the observation house to provide reference total-field magnetic measurements at corresponding timestamps. To validate consistency in error calibration parameter estimation, the test was repeated twice. The acquired experimental data were subsequently processed using the error calibration framework detailed in Section 3 to calibrate the fluxgate sensors.

Table 1 reports the standard deviations of the computed total field magnitudes for all four fluxgates before and after calibration across both test trials. Results indicate that post-calibration standard deviations were consistently reduced below 2 nT for all sensors, confirming robust calibration efficacy.

Table 1: Standard deviation of computed total magnetic field data before vs. after calibration (unit: nT).

Test	Fluxg	gate 1	Fluxgate 2		Fluxgate 3		Fluxgate 4	
group	Before	After	Before	After	Before	After	Before	After
Test 1	59.00	0.65	54.76	1.30	124.60	1.02	174.69	1.43
Test 2	59.86	0.46	54.39	0.54	124.55	0.40	175.06	0.42

# 4.2 Filed calibration test for Misalignment errors between fluxgate sensors

Within the absolute geomagnetic observation house of the seismic monitoring station, the magnetic gradient tensor measurement array was mounted on a non-magnetic turntable. The turntable was rotated  $360^{\circ}$  around the x-, y-, and z-axes (defined relative to the fluxgate array coordinate system) in  $15^{\circ}$  increments, yielding 72 distinct orientations of the fluxgate array. The triaxial readings of each fluxgate sensor were recorded at every orientation. Additionally, a static data acquisition experiment was conducted to establish baseline noise levels between fluxgates after misalignment calibration as a reference. The acquired data were processed using the error calibration methodology detailed in Section 3

To quantitatively evaluate calibration performance, Table 2 presents the Root Mean Squared Differences (RMSD) of triaxial readings between Fluxgate 1 and Fluxgates 2–4 before and after calibration, alongside RMSD values from static conditions. The RMSD is defined as:

$$RMSD_{jk} = \sqrt{\frac{1}{n} \sum_{i=1}^{n} \left( B_{jk}^{i} - B_{1k}^{i} \right)^{2}}; i = 2, 3, 4; j = x, y, z$$
(36)

Where  $B_{ik}^i$  denotes the k-axis component reading of the j-th fluxgate in the i-th experimental dataset.

Table 2: RMSD o	of triaxial read	ings between	fluxgates	before vs.	after	calibration	(unit: $nT$ ).

Calibration	ion RMSD between Fluxgate 1 & 2			RMSD between Fluxgate 1 & 3			RMSD between Fluxgate 1 & 4		
test	x-axis	y-axis	z-axis	<i>x</i> -axis	y-axis	z-axis	x-axis	y-axis	z-axis
Before	425.94	394.19	400.66	629.06	401.46	301.94	576.62	409.39	484.59
After	24.34	42.86	28.36	17.30	20.33	19.79	17.16	20.46	23.00
Static	19.66	29.12	13.48	8.47	10.78	8.83	2.76	6.87	10.52

Table 2 onfirms that post-calibration RMSD values of triaxial readings between fluxgates were significantly reduced, all falling below 45 nT. These values exhibited minimal divergence from RMSD values measured under static conditions, indicating effective misalignment error calibration.

# 4.3 Filed calibration test for Misalignment errors between inertial navigation system and fluxgate sensors

To ensure optimal GPS antenna signal reception for maintaining the precision of INS (CGI-430, Shanghai Huace Navigation Technology Ltd.) attitude measurements, the experiment was conducted in a relatively open and magnetically stable calibration but within a seismic monitoring station.

The INS and MGT measurement array were rigidly connected via acrylic structural components to eliminate relative motion between the fluxgate sensors and the INS. This assembly was mounted on a non-magnetic turntable using nylon screws. The entire hardware system was rotated 360° about two distinct axes defined in the INS and fluxgate coordinate frames, with a rotational step size of 10°, yielding 72 datasets. Attitude readings from the INS and magnetic vector measurements from the fluxgates were synchronously recorded via a data acquisition unit at each orientation. The acquired data were processed using the misalignment error calibration methodology detailed in Section 3.

To quantitatively evaluate the calibration efficacy, the Standard Deviations (STD) of the triaxial magnetic readings (reflecting fluctuation levels) were calculated. As summarized in Table 3, the precalibration standard deviations approximate 3,000 nT across all three axes. Post-calibration, these values decreased to approximately 300 nT, confirming that the INS-derived attitude data now accurately represent the fluxgate's orientation. This validates the method's effectiveness in calibrating INS-fluxgate misalignment errors.

Table 3: STD of triaxial readings transformed to unified coordinate frame before vs. after calibration (unit: nT).

Calibration test	STD of x-axis readings	STD of <i>y</i> -axis readings	STD of z-axis readings
Before	3355.33	3037.14	2317.77
After	394.54	555.99	164.93

# 5. Conclusion

This paper proposes a comprehensive error calibration methodology for magnetic gradient tensor detection systems. The key innovations distinguishing this work from prior research include: The theoretical demonstration of inherent constraint relationships between fluxgate sensors and INS measurements within stable uniform vector fields, enabling a new misalignment calibration approach between these heterogeneous sensors.

Field validation experiments conducted at Yingcheng Seismic Monitoring Station (Hubei Earthquake Agency) confirmed the method's efficacy. Post-calibration results demonstrated: Standard deviation of fluxgate-derived total field reduced to < 2 nT (pre-calibration: 54.36–175.06 nT); RMS differences between fluxgate triaxial readings decreased to < 45 nT (pre-calibration: 301.94–629.06 nT); Standard deviation of coordinate-transformed triaxial readings lowered to < 580 nT (pre-calibration: 2,317.77–3,355.33 nT).

These advancements significantly enhance magnetic measurement precision, demonstrating substantial potential for applications in geomagnetic matching navigation and related fields.

#### References

- [1] Xu N, Wang L, Wu T, et al. An innovative PSO-ICCP matching algorithm for geomagnetic navigation [J]. Measurement, 2022, 193: 110958.
- [2] Chen Z, Liu K, Zhang Q, et al. Geomagnetic vector pattern recognition navigation method based on probabilistic neural network[J]. IEEE Transactions on Geoscience and Remote Sensing, 2023, 61: 1-8.
- [3] Quan S, Zhou Y, Zhao S, et al. An inertial constraint-aided geomagnetic matching algorithm for underwater navigation[J]. Measurement, 2025: 118156.
- [4] Zhang X, Chen Z, Chi C, et al. Heuristic Geomagnetic Matching Algorithm Based on Geomagnetic Characteristic Parameters[J]. IEEE Transactions on Instrumentation and Measurement, 2025.
- [5] Cuenca A, Moncayo H, Gavilanez G. Artificial intelligence-assisted geomagnetic navigation framework[J]. IEEE Transactions on Aerospace and Electronic Systems, 2024.
- [6] Zheng X, Tian Y, Wang B. A magnetic gradient tensor based method for UXO detection on movable platform[J]. IEEE Transactions on Geoscience and Remote Sensing, 2023, 61: 1-9.
- [7] Du G, Wang Y, Wang G, et al. A robust calibration and adaptive multipair of magnetic gradient tensors localization method for magnetic anomaly detection[J]. IEEE Transactions on Geoscience and Remote Sensing, 2023, 61: 1-14.
- [8] Li Q, Shi Z, Li Z, et al. Preferred configuration and detection limits estimation of magnetic gradient tensor system[J]. IEEE Transactions on Instrumentation and Measurement, 2021, 70: 1-14.
- [9] Yang R, Wang H, Luo W, et al. Cumulative Error Calibration of Fluxgate Sensor Considering Temperature Effects[J]. IEEE Transactions on Instrumentation and Measurement, 2024.
- [10] Ren Y, Wang Y, Wang M, et al. A measuring system for well logging attitude and a method of sensor calibration[J]. sensors, 2014, 14(5): 9256-9270.
- [11] Farsimadan A, Behnamgol V. Magnetometer Calibration Using Ellipsoid Fitting Method[J]. Transactions on Machine Intelligence, 2019, 2(1): 10-19.
- [12] Yan Y, Ma Y, Liu J. Analysis and correction of the magnetometer's position error in a cross-shaped magnetic tensor gradiometer[J]. Sensors, 2020, 20(5): 1290.
- [13] Kubík J, Janošek M, Ripka P. Low-power fluxgate sensor signal processing using gated differential integrato[J]r. Sensor Letters, 2007, 5(1): 149-152.
- [14] Pang H, Zhu X J, Pan M, et al. Misalignment calibration of geomagnetic vector measurement system using parallelepiped frame rotation method[J]. Journal of Magnetism and Magnetic Materials, 2016, 419: 309-316.
- [15] Li X, Li Z. A new calibration method for tri-axial field sensors in strap-down navigation systems[J]. Measurement Science and technology, 2012, 23(10): 105105.
- [16] Li Q, Shi Z, Li Z, et al. Magnetic object positioning based on second-order magnetic gradient tensor system[J]. IEEE Sensors Journal, 2021, 21(16): 18237-18248.
- [17] Xu L, Zhang N, Fang L, et al. Simulation Analysis of Magnetic Gradient Full-Tensor Measurement System[J]. Mathematical Problems in Engineering, 2021, 2021(1): 6688364.
- [18] Milligan T. More applications of Euler rotation angles[J]. IEEE Antennas and Propagation Magazine, 1999, 41(4): 78-83.
- [19] Ranganathan A. The levenberg-marquardt algorithm[J]. Tutoral on LM algorithm, 2004, 11(1): 101-110.
- [20] Dai J S. Euler–Rodrigues formula variations, quaternion conjugation and intrinsic connections[J]. Mechanism and Machine Theory, 2015, 92: 144-152.